Spectrochimica Acta Part A: Molecular and Biomolecular Spectroscopy 343 (2025) 126564

Contents lists available at ScienceDirect

Spectrochimica Acta Part A:
Molecular and Biomolecular Spectroscopy

journal homepage: www.journals.elsevier.com/spectrochimica-acta-part-a-molecular-and-biomolecular-spectroscopy

Raman spectral analyses to investigate the physiological and metabolic development of a 3D hepatocellular carcinoma model

M.G. Rizzo [a], C. Corsaro [b], S. Marrara [b], V. Crupi [b], S. Conoci [a,c,d], F. Neri [b], E. Fazio [b,*]

[a] Department of Chemical Sciences, Biological, Pharmaceutical and Environmental, University of Messina, Viale F. Stagno d'Alcontres, 31, Messina, 98166, Italy
[b] Department of Mathematics and Computer Sciences, Physical Sciences and Earth Sciences, University of Messina, Viale F. Stagno d'Alcontres, 31, Messina, 98166, Italy
[c] CNR-DSFTM, URT LabSens Beyond Nano Messina, Viale F. Stagno d'Alcontres, 31, Mesina, 98166, Italy
[d] Department of Chemistry G. Ciamician, University of Bologna, Via Francesco Selmi 2, Bologna, 40126, Italy

GRAPHICAL ABSTRACT

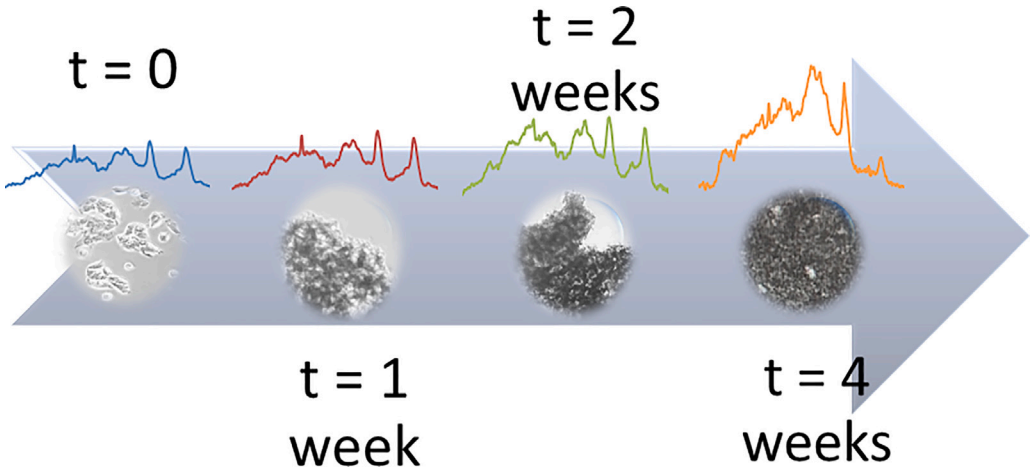

HIGHLIGHTS

- Successful generation of a 3D model for HepG2 cells.
- Characterization of 3D model evolution by micro-Raman spectroscopy.
- Raman changes as index of tumor physiological evolution.

ARTICLE INFO

Keywords:
Hepatocellular carcinoma
3D cell model
Tumor microenvironment
Raman spectroscopy

ABSTRACT

Three-dimensional (3D) cell culture models are increasingly attracting interest as powerful tools to recapitulate the in vivo tumor microenvironment, offering a more physiologically relevant alternative to traditional two-dimensional (2D) cultures. In this work, a 3D hepatocellular carcinoma (HCC) model using the HepG2 cell line was recreated and characterized over time. Gene expression analyses revealed changes in markers of proliferation (PCNA, Ki-67), differentiation (AFP), hypoxia (HIF-1α) and apoptotic regulators (BBC3), associated

* Corresponding author.
E-mail address: enfazio@unime.it (E. Fazio).

https://doi.org/10.1016/j.saa.2025.126564
Received 16 March 2025; Received in revised form 30 May 2025; Accepted 11 June 2025
Available online 24 June 2025

Physiological markers

to the key adaptive phases of tumor development. Results exhibit a marked cells accumulation in the G0/G1 phase, indicative of a transition to quiescence. Raman analysis assessed biochemical composition and cellular response over time, allowing a non-invasive monitoring of metabolic states by detecting specific molecular vibrations. A clear correlation between the Raman spectral changes and the key genes involved in proliferation (PCNA, KI-67), differentiation (AFP), hypoxia (HIF-1α and apoptosis (BBC3) were found, so providing insights into the physiological evolution of 3D HepG2 spheroids. Thus, Raman approach could be a valuable tool to follow in real-time tumor adaptation and microenvironmental stress responses.

1. Introduction

Hepatocellular carcinoma (HCC) is the most common form of liver cancer and accounts for 90% of cases [1]. Pathogenic steps of HCC usually encompass liver injury, chronic inflammation, fibrosis, cirrhosis, and liver cancer [2,3]. The complex and diverse pathogenesis of HCC, coupled with the limited efficacy of current therapeutic approaches, underscores the urgency of developing advanced preclinical models to better understand its pathophysiology and identify novel therapeutic targets. In this context, tumor progression is tightly regulated by a dynamic interplay between proliferative signals, metabolic shifts, and microenvironmental pressures, which can only be effectively captured in physiologically relevant models [4].

The development of three-dimensional (3D) models, including spheroids and organoids, is revolutionizing biomedical research by offering more reliable alternatives to traditional two-dimensional (2D) cultures [5]. Unlike 2D cultures, 3D systems allow cells to grow and interact in all dimensions, better reflecting the tumor biologic dynamics and its metabolic plasticity, a key feature in cancer progression involving adaptive shifts in energy production, redox balance, and extracellular matrix remodeling. Thus, 3D models effectively mimic key aspects of tumor physiology, such as hypoxia, nutrient diffusion limitations, and cell–cell interactions, providing deeper insights into cancer progression and therapeutic responses [6]. Specifically, 3D cultures derived from hepatocellular carcinoma can be successfully replicate the hallmarks of HCC, including altered proliferation and apoptotic signaling pathways [7,8].

Recent evidence has explored the structural integrity, cell viability and gene expression of HCC spheroids. For example, Martina Štampar et al. [9] reported that HepG2 spheroids, formed by forced flotation method with initial densities of 3000 and 6000 cells, were analyzed for 6–12 days to follow growth dynamics, surface parameters and viability changes. Key liver markers, proliferation indicators and genes involved in metabolism I/II phases were assessed using real-time quantitative PCR. Despite their advantages, 3D models present significant challenges in maintaining functional viability over extended periods of culture. Monitoring the physiological and molecular status of 3D models in real time is therefore crucial to validate their relevance and ensure their reproducibility [10].

HepG2 cell proliferation is generally assessed using markers like PCNA (Proliferation Cell Nuclear Antigen) and Ki-67. Both markers indicate cell cycle activity, with Ki-67 being more specific for active proliferation. Recent studies show that Ki-67 levels correlate with tumor aggressiveness and prognosis in various cancers, including liver cancer. The expression levels of Ki-67 and PCNA are correlated with tumor growth and patient prognosis. High levels of these proteins typically indicate increased cellular proliferation, making them valuable targets for therapeutic interventions and diagnostic assessments. Using 3D models derived from HCC cell lines allows researchers to study the spatial organization and interactions of these proteins within a more physiologically relevant environment. This approach can reveal how lipid distributions change in relation to Ki-67 expression during different phases of the cell cycle, providing insights into cancer biology and potential therapeutic targets.

Raman spectroscopy has emerged as a powerful tool for analyzing the biochemical composition of cancer cells. In studies involving HCC, significant spectral differences have been observed in terms of biochemical composition and cellular changes. Raman spectra of HCC cells exhibit distinct peaks that correlate with nucleic acids, proteins, and lipids. Notably, peaks at approximately 782, 1094, 1335, and 1578 cm^{-1} indicate a higher presence of DNA in cancerous cells compared to normal cells. In addition, increased intensity in specific spectral regions suggests enhanced lipid and DNA content within HCC tissues, which may reflect malignancy and cellular proliferation [11]. Raman spectroscopy identifies specific HCC biomarkers, such as differences in carotenoid, amino acid, lipid, and nucleic acid levels. For example, peaks related to nucleic acids and saccharides are higher in advanced stages of HCC [12]. This biochemical mapping allows researchers to visualize changes in molecular composition over time, providing insights into tumor progression and response to therapies. However, some efforts are necessary to analyze the correlation between the molecular interactions and structural characteristics that can be detected through Raman spectroscopy, particularly in relation to cancer cell proliferation and corresponding gene expression. Hence, Raman spectroscopy has the potential to differentiate the unique protein marker expression features of HCC cell lines that represent hepatocyte-like and mesenchymal-like subgroups [13]. Despite advances in tumor modeling and molecular diagnostics, current approaches often lack the ability to longitudinally monitor tumor development and cellular dynamics within 3D models beyond short time frames (typically up to 15 days). Moreover, existing methods rarely integrate biochemical profiling with gene expression data to provide a comprehensive and temporally resolved picture of tumor biology.

The main challenges addressed in this work include (i) extending the monitoring period of 3D tumor models to four weeks to assess long-term stability and functional integrity, (ii) establishing a direct correlation between Raman spectral changes and key gene expression markers related to proliferation (PCNA, Ki-67), differentiation (AFP), hypoxia (HIF−1α) and apoptosis (BBC3), and (iii) developing a dual-modality approach that combines non-invasive biochemical sensing with molecular biology techniques.

First, we chose to monitor the developed 3D model for longer time (up to four weeks) with respect to literature data (about 15 days) in order to assess stability, structural and functional cells integrity. This innovative integration enables more accurate tracking of tumor progression and cellular states, potentially improving early diagnosis, patient stratification, and personalized treatment strategies. By overcoming the limitations of short-term monitoring and single-modality analysis, our approach opens new avenues for dynamic, multi-parametric assessment of tumor models and therapeutic responses.

Hence, a key innovation of this study is the detailed mapping of specific Raman spectral peaks to the expression of pivotal genes involved in tumor progression and cellular fate decisions. For example, we expected that Raman peaks in the 750–790 cm^{-1} and 1085–1095 cm^{-1} ranges, corresponding to DNA/RNA backbone vibrations, increase in intensity in parallel with elevated PCNA and Ki-67 expression, reflecting heightened cellular proliferation activity. On the other hand, apoptosis marker BBC3 (also known as PUMA) correlates with Raman peaks related to nucleic acid fragmentation and changes in protein conformation, such as those observed near 1265 cm^{-1} (amide III) and 1585 cm^{-1} (adenine/guanine vibrations). These spectral changes reflect the activation of programmed cell death pathways within the tumor model.

Table 1
Gene target used in qRT-PCR.

Protein name	Target gene	Protein function	Forward	Reverse
Proliferating cell nuclear antigen	PCNA	DNA replication control (increases the processability of the polymerase)	CAAGTAATGTCG ATAAAGAGGAGG	GTGTCACCGTT GAAGAGAGTGG
Proliferation marker protein	KI67	Encodes a nuclear antigen in all phase of the cell cycle (except G0)	GAAAGAGTGGC AACCTGCCTTC	GCACCAAGTTTT ACTACATCTGCC
Alpha-fetoprotein	AFP	Regulates cell growth	GCAGAGGAGAT GTGCTGGATTG	CGTGGTCAGTTT GCAGCATTCTG
Hypoxia-inducible factor 1-alpha	HIF-1α	Mediates cellular adaptation to hypoxic conditions	TATGAGCCAGAA GAACTTTTAGGC	CACCTCTTTTGG CAAGCATCCTG
Bcl-2-binding component 3	BBC3	Causes apoptosis	ACGACCTCAAC GCACAGTACGA	CCTAATTGGGC TCCATCTCGGG

2. Experimental section

2.1. Cells culture

Caucasian male Homo sapiens (human) hepatocellular carcinoma cell line (HepG2; ATCC, HB-8065, Manassas, USA) was used in this study. HepG2 cells were maintained in 75 cm^2 culture flasks containing Dulbecco's modified Eagle's medium (DMEM) supplemented with 4.5 g/L glucose and 10 g/L L-glutamine (G7513, Merk Life Science S.r.l., Milan, Italy) containing 100 mL/L foetal calf serum (F7524, FBS, Merk Life Science S.r.l., Milan, Italy), and 1% penicillin/streptomycin/amphotericin (A5955, Merk Life Science S.r.l., Milan, Italy). The culture medium was renewed by a fresh medium every 3 days and cells were sub-cultured.

2.2. 3D human hepatocellular carcinoma model generation

The 3D spheroid models were generated using the hanging drop method as reported in Ref. [14,15]. The model used was obtained from an initial cell density of 5×10^4 cells/mL, as reported in previous studies [9]. Droplets were monitored at specific time points (1, 3, 4 weeks). Each condition was tested in triplicate and repeated in three independent experiments to ensure reproducibility.

2.3. Gene expression profile of the 3D model from HepG2

To investigate the gene expression levels during the development of the 3D model, PCNA, Ki-67, AFP, HIF-1α, BBC3 genes were analyzed by quantitative real-time PCR. Total RNA was extracted from samples incubated for 1, 3, and 4 weeks using TRIzol reagent (Invitrogen, Carlsbad, CA, USA) according to the manufacturer's instructions. RNAs samples were quantify using a ND-1000 UV spectrophotometer (Nanodrop, Wilmington, DE). qRT-PCR was carried out in a 20 μL reaction mixture containing 1 μL of cDNA preparation, 0.5 mM of each forward and reverse primers and 10 μL of SsoAdvanced universal SYBR1 Green supermix (2X) (Bio-Rad Laboratories, Hercules, CA, USA). The amplification was carried out using a 7500 Fast Real-Time PCR System. A melting curve analysis was performed using the instrument default settings. For this study, gene expression data were analyzed by the $2^{-\Delta\Delta Ct}$ method and presented as fold change relative to day 1 [16]. Gene target used are reported in Table 1.

2.4. SEM and micro-Raman characterizations

Micro-Raman spectroscopy has been used to identify specific biomarker detection of carcinoma and to highlight the differences between the HepG2 cells and their biological diversity, also looking to cells morphological changes followed acquiring high resolution Scanning Electron Microscopy (SEM) images. Micro-Raman measurements were carried out by using the XploRa Horiba spectrometer after the transfer of the cells onto CaF_2 substrates, chosen for their excellent transmission in UV, visible, and IR ranges. CaF_2 substrates were washed twice with phosphate-buffered saline without calcium and magnesium and fixed with 4% formalin for 20 min. After two washings in ultrapure water, the sample was air-dried at room temperature. HepG2 3D samples were also tested in a near-liquid state to obtain Raman spectral features more representative of the liquid condition. However, in this case, the Raman signal was relatively weak, despite the spectral features being comparable to those of the dried samples (not shown). For these measurements, a holder designed to accommodate a standard 10 mm × 10 mm cuvette to facilitate liquid sample analysis. Clear Raman signals were collected by adopting the following conditions: 532 nm laser excitation wavelength, laser power lower than 1 mW, a laser spot size of 1–2 μm, an integration time between 30 and 60 s, changing the accumulation number (1–3) to maximize the signal-to-noise ratio. The Raman backscattered light was spectrally separated using 600 lines per mm grating and detected with a CCD Camera (Deep Cooled Camera, cooled to −60 °C). To align the spectra, the system was calibrated daily to the spectral line of crystalline silicon at 521 cm^{-1}. For background subtraction, a spectrum was recorded on the surface of the CaF_2 substrate and all the spectra were normalized to their own integration time. For some spectra, to remove the fluorescence contribution, the baseline was corrected by applying a polynomial fitting. Preliminarily, in order to evaluate intracellular variability, Raman scattering measurements were performed, repositioning laser spots on several different locations of the sample surface; the results presented here are representative of a large set of measurements. Moreover, we tested the samples surface homogeneity (spot-to-spot reproducibility) by acquiring micro-Raman maps. The maps were recorded, using x-y motorized tables, on an area of 30 μm × 30 μm with step of 5 μm using a 50× objective. Furthermore, environmental factors such as temperature, humidity, and laser power stability during measurements, were recorded and controlled as these could affect Raman spectra. Scanning Electron Microscopy (SEM) images were collected using a Zeiss field emission microscopy. SEM analyses were carried out with a Zeiss-Gemini 2 electron microscope, operating at about 20 kV and a working distance of 13 mm.

3D models were stained using a live/dead viability kit with SYTO 9 and Propidium Iodide (PI) as fluorescent probes. The staining solution was prepared in PBS and directly added to the 3D culture to achieve final concentrations of 5 μM SYTO 9 and 30 μM PI. Spheroids were incubated for 20–30 min at 37 °C in the dark. Following staining, spheroids were gently washed with PBS and transferred to glass-bottom dishes for imaging. Images were acquired using a Leica confocal microscope. SYTO 9 was excited at 488 nm and detected within the 500–550 nm range, while PI was excited at 561 nm and detected within the 570–620 nm range.

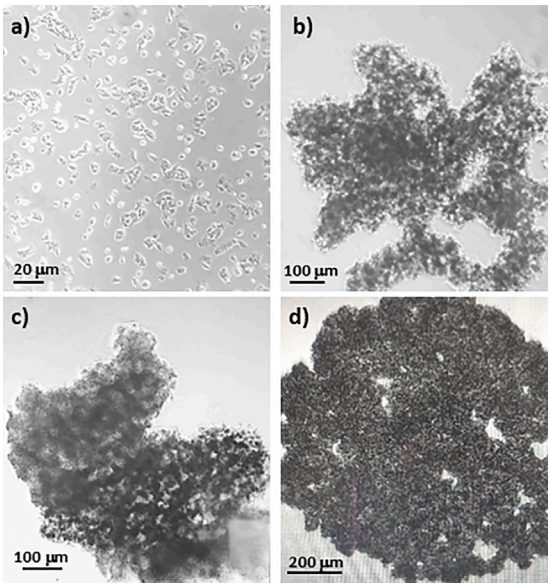

Fig. 1. Representative images of 3D model development at: (a) t = 0; (b) 1 week; (c) 2 weeks and (d) 4 weeks of incubation.

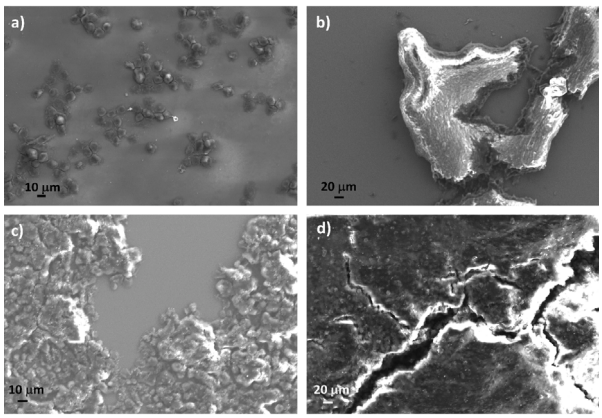

Fig. 2. SEM images of the 3D HCC-MOSs cells at different development times: (a) t = 0; (b) 1 week; (c) 3 weeks and (d) 4 weeks.

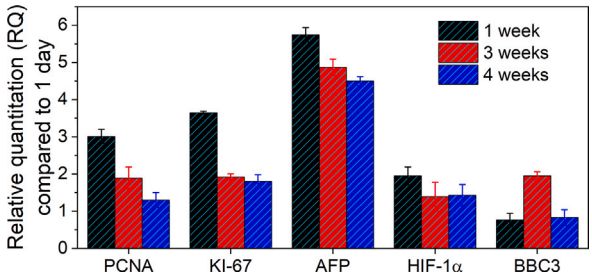

Fig. 3. Gene Expression profile of the 3D model from HepG2. Data expressed as relative quantitation (RQ) and Glyceraldehyde 3-phosphate dehydrogenase (GAPDH) was used as a control for normalization. The data were derived from three independent experiments conducted in triplicate.

3. Results

3.1. Conventional optical and SEM characterizations

The hanging drops were monitored daily throughout the incubation period to observe the formation of cell sheets or aggregates. Some representative optical images for each aggregation stage are shown in Fig. 1. These images were captured using a Leica DMi1 inverted microscope equipped with a FLEXACAM C1 12 MP stand-alone camera (Leica Camera AG, Wetzlar, Germany).

The corresponding SEM images are shown in Fig. 2. In the early stage, the nearly-circular cells, about 10 µm in diameter, occur in clusters uniformly distributed (Figs. 1a and 2a). Instead, after 1 week from the preparation (Figs. 1b, 2b), the cells in the spheroids develop in a peninsula-like structure, gradually moving from denser and well-structured areas to less dense ones, as if the evolution process had not yet been completed. In the next times (after 3 and 4 weeks from the preparation), cells gradually formed large, spheroidal colonies along the culture process (Figs. 1c,d and 2c,d). In addition, extracellular materials on the surfaces of HepG2 cells as well as small cracks (presumably caused by dehydration during sample preparation for SEM) were also observed. In any case, the cells in 3D cultures show tighter interactions with each other compared to the flat and dispersed appearance of cells in 2D cultures [17,18].

The observed formation of multicellular spheroids significantly impacts HepG2 cell behavior by creating an in vivo-like microenvironment that more closely represents normal cellular function. This 3D environment leads to increased cell-to-cell interactions and mimics the architecture of natural organs and tissues. As a proven fact, we observed an evolution versus a porous structure with interconnected pores which is crucial to support cell migration, proliferation, and nutrient/waste exchange [19].

3.2. Gene expression profile of the 3D model from HepG2

The temporal analysis of gene expression in the HepG2 3D cell model reveals distinct phases of cellular activity over time. In Fig. 3 are reported gene expression profiles of the 3D HepG2 model. PCNA and Ki-67 (proliferation markers), show an increase at 1 week, indicating an initial phase of cell division. In particular, the PCNA expression at 1 week was 3.015 ± 0.187, at 3 weeks (1.891 ± 0.298) and 4 weeks (1.300 ± 0.200). Ki-67 expression was highest at 1 week (3.649 ± 0.036), decreasing at 3 weeks (1.921 ± 0.084) and stabilizing at 4 weeks (1.800 ± 0.180). The AFP (differentiation marker) showed at 3 weeks expression levels of 4.866 ± 0.219 that slightly decreases at 4 weeks (4.500 ± 0.120). AFP expression at 1 week was 5.741 ± 0.194, indicating an initial high expression.

Regarding hypoxia-related responses, HIF-1α expression remained stable all time points, suggesting an adaptation to the low-oxygen microenvironment. Expression values were 1.949 ± 0.238 at 1 week, 1.389 ± 0.387 at 3 weeks, and 1.430 ± 0.290 at 4 weeks. Finally, the BBC3 (pro-apoptotic marker) showed an increase at 3 weeks (1.950 ± 0.114) compared to 1 week (0.764 ± 0.183), followed by stabilization at 4 weeks (0.830 ± 0.210). Overall, this temporal gene expression profile delineates a structured transition from proliferation to differentiation and subsequent stabilization, underscoring the ability of the 3D HepG2 model to recapitulate key physiological phases of tumor microenvironment adaptation. Hence, 3D models promotes apoptosis while hypoxia and environment confer resistance to apoptosis by upregulating protective mechanisms.

Confocal images, presented in Fig. 4, display intense green fluorescence alongside basal red fluorescence, indicating that the majority of cells retained membrane integrity and remained viable in both peripheral and central regions. These findings demonstrate the presence of a structurally stable and metabolically active spheroid under chronic hypoxic conditions.

3.3. Micro-Raman characterization

Fig. 5 shows Raman spectra of the investigated cells after only the background subtraction and an entire optical image of the 3D cells

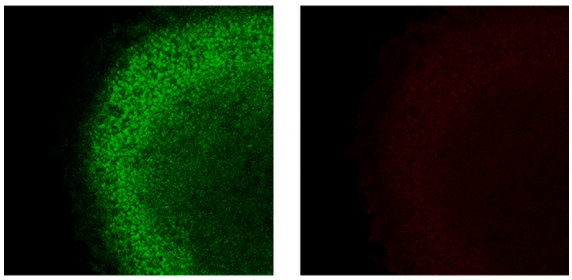

Fig. 4. Live/Dead staining of 3D spheroid model acquired by confocal microscopy. SYTO 9 is a green fluorescent nucleic stain that penetrates both living and dead cells, binding to DNA and RNA and displaying intense green fluorescence. Instead, propidium Iodide (PI) is a red fluorescent dye that penetrates only cells with compromised membranes, typically dead or damaged cells. When used in combination with SYTO 9, PI competes for DNA binding and reduces the green fluorescence of SYTO 9 in dead cells, thus allowing live (green) cells to be distinguished from dead (red) cells.

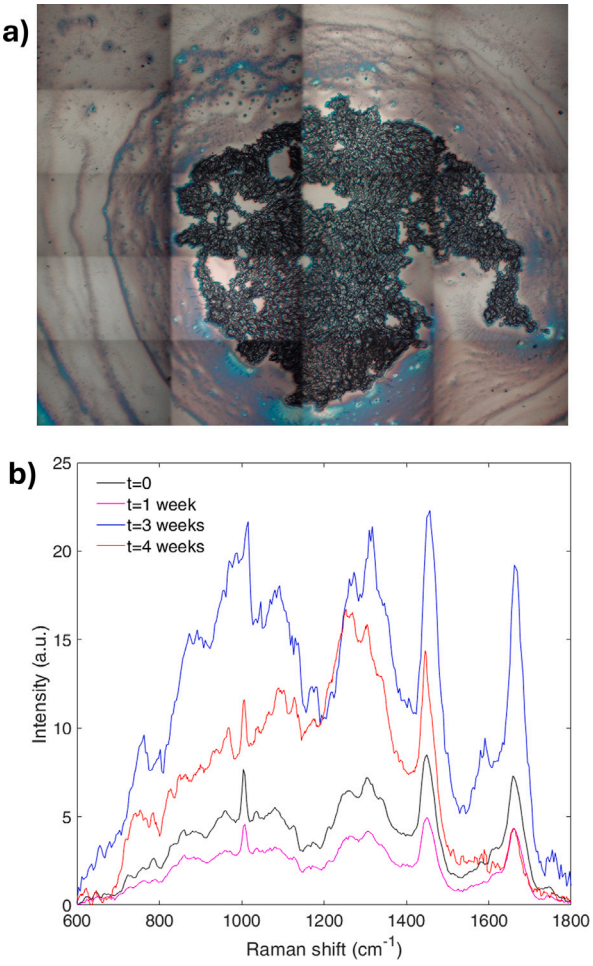

Fig. 5. Optical mosaic reconstruction of the 3D model (a) and Raman spectra of the investigated cells at different incubation time (b).

in the fourth week of incubation. This image was acquired with the assistance of HORIBA's EasyNavTM package, integrated in the LabSPEC 6 software (HORIBA Jobin Yvon, Edison, NJ, United States). This approach allows a mosaic reconstruction by enabling fast imaging of large sample areas by video stitching. So, we had the possibility to visualize the entire sample and to select different points on which we have carried out Raman measurements.

We outline that to account for typical variations in overall intensity due to experimental factors such as laser power fluctuations, sample

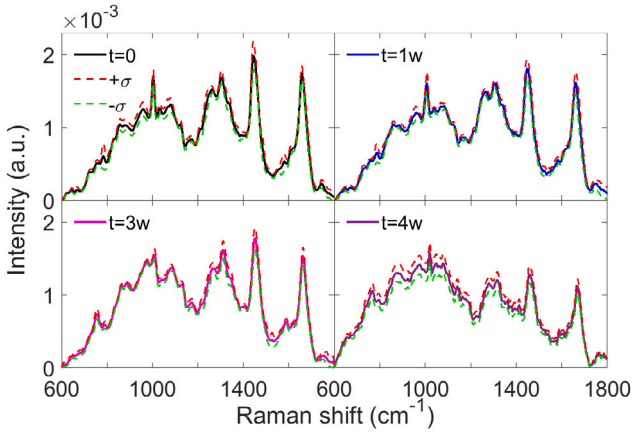

Fig. 6. Averaged Raman spectra normalized to the total area (solid lines) and corresponding standard deviation (dashed lines) at: t = 0, 1 week, 3 weeks and 4 weeks of incubation.

thickness, or cell density, Raman spectra were normalized to the total spectral area. Normalization of the Raman spectra of 3D HepG2 cell models to the total spectral area did not alter the trends observed in the non-normalized spectra. This indicates that the underlying biochemical changes reflected in the spectra are robust and consistent. Thus, the observed biochemical composition changes associated with growth and development of the 3D HepG2 cell cultures are sufficiently distinct that normalization preserves the spectral trends (see Fig. 6), confirming that the spectral differences are biologically meaningful rather than artifacts of measurement variability. This is consistent with the stable proliferation and phenotypic changes reported in 3D HepG2 models, where spectral features reflect genuine cellular and microenvironmental alterations rather than noise. In details, Raman spectra of HePG2 cells at t = 0 (start of incubation) and after 1, 3, 4 weeks from the preparation show a similar spectral pattern. All spectra have distinct Raman bands centered at about 860, 1085, 1260–1370, and 1585 cm^{-1}, corresponding to the vibrational modes of the nucleic acid. Other intense peaks were identified at 1005 and 1265 cm^{-1}, corresponding to the phenylalanine and Amide III bands, respectively. A prominent peak at 1445 cm^{-1}, related to proteins/lipids vibrational bonds, and an intense Amide I band at 1660 cm^{-1} were also evident. A detailed band assignment of the vibrational modes of the major biomolecules (nucleic acids, proteins, lipids, and carbohydrates) characterizing the cells are summarized in Table 2.

Comparing all Raman profiles, we observe that several spectra are close to one another, but with some slight differences. Principal Component Analysis (PCA) is performed on the spectral dataset to reduce the complex spectral data into principal components that capture the most significant variations related to time-dependent cellular changes (Fig. 7).

Although the complexity of the 3D data and the subtle biochemical changes occurring at different times can limit the ability of PCA, it quite clearly resolves distinct temporal patterns in the spectra. We outline that Raman spectra were collected over a 30 μm × 30 μm area of each sample and the points were spaced at 5 μm along the x and y directions. So, the analysis of these Raman spectra allowed the detection (if present) of some spectral differences as a function of the sampling point. Raman spectra recorded at different positions were similar, pointing out for the absence of evident intracellular variability, establishing that proteins and lipids are homogeneously distributed.

The comparative analysis evidences that the main spectral differences (in terms of intensity changes and Raman shifts) are associated to phenylalanine (encoded by DNA via mRNA, essential for protein synthesis and may influence growth and DNA/RNA synthesis in HepG2 cells) and proteins/lipids vibrational bonds during the

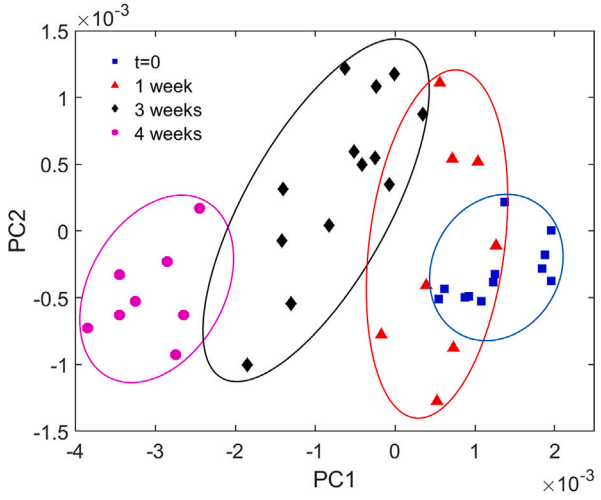

Fig. 7. Score plot of the PCA showing a good clustering among Raman spectra acquired on 3D HepG2 cell culture at t = 0, 1 week, 3 weeks and 4 weeks of incubation.

proliferation phase. These changes are linked with reactive oxygen species and hydroxyproline levels in proliferating human hepatocytes (ProliHHs) [20]. Specifically, the sharp bands in the 990–1025 cm^{-1} range originate from the ring breathing modes of phenylalanine within protein species. Their intensity is relatively low after 3–4 weeks, with a trend similar to that observed in cells treated with fatty acids for five days [21]. This suggests that lipid droplets have lipoproteins on their surfaces. Specifically, we have followed the ratio of the Raman peak intensity ascribed to lipid deformation mode (at about 1310 cm^{-1}) to that of the Amide III band (at about 1265 cm^{-1}). It was found that the (Lipid/Amide III) intensity ratio decreases from 1.11 to 1.03. Interestingly, the intensities variations of the features centered at about 1085 cm^{-1} and 1585 cm^{-1} are more pronounced after 3 weeks. As reported in literature, the intensities of these two contributions are proportional to the concentration of Alpha-fetoprotein (AFP) [22], which can regulate the growth of HepG2 cells, interacting with the retinoic acid receptor (RAR) and preventing it from entering the nucleus. These spectral variations correspond to shifts in cellular metabolism, a crucial physiological adaptation that enables tumor cells to optimize energy production and survival under microenvironmental stress [23].

Finally, Raman features ascribed to nuclear proteins (700–950 cm^{-1}) may be associated to the well-known marker protein Ki-67, used to identify proliferating cells and then as a prominent cancer marker [29], while the main Raman features in the 1200–1400 cm^{-1} range are ascribed to hypoxia-induced extracellular vesicles (EV) proteins. We remember that EVs production rates and composition are supposed to be one of the mechanisms by which cancer cells respond to hypoxic stimulus. Hypoxic stress leads to multiple changes both inside tumor tissue and in tumor microenvironment, causing better adaptation of cancer to low oxygen levels [30]. Moreover, HIF-1α, accumulated in the nucleus due to hypoxia or external stimulation, contributes to induce proliferation and metabolic changes. Raman evidence of this occurrence is the broad band in the 800–1100 cm^{-1} range after three weeks. Finally, the shift of the Raman peak positions to lower wavenumbers after 4 weeks indicates a decrement of the cell viability; plausibly adenosine can inhibit HepG2 cell proliferation via induction of apoptosis [31].

4. Discussion

Using human hepatocarcinoma cell lines like HepG2 in vitro models offers several benefits, including ease of culture, unlimited lifespan, stable phenotype, high availability, low costs, and avoidance of inter-donor variations. When cultured in a 3D arrangement, the liver-like functionality of HepG2 cells is enhanced, leading to increased cell-to-cell contacts, improved intercellular communication, and changes in the protein expression and metabolic status of the cells. Specifically, genes related to the extracellular matrix, cytoskeleton, and cell adhesion have higher expression in 2D cultures. Instead, HepG2 cells in 3D cultures upregulate genes involved in liver-specific xenobiotic and lipid metabolism [32].

The results obtained from our developed HepG2 3D model reveal a complex pattern of cellular adaptation to the three-dimensional growth environment. Temporal analysis of gene expression markers and Raman profiles highlight distinct phases of proliferation, differentiation, and apoptosis. The initial surge (first week) in the expression of proliferation markers PCNA and Ki-67 and the correlated Raman features (in terms of protein, lipids etc.) indicates intense cellular activity required for the establishment of the 3D structure. Ki-67 encodes for a very important nuclear antigen that is present in the active phases of the cell cycle, except the G0 phase. Instead, PCNA is a nuclear antigen of proliferating cells, a protein essential for DNA replication, so a lack of its expression induces cell cycle arrest in S G2/M phase [9]. Proliferation phase is followed by a decrease in PCNA and Ki-67 gene expression, which may be attributed to the limited diffusion of oxygen and nutrients in the dense three-dimensional structure and/or to a DNA-damage accumulation in HCC cells [33]. Glucose deprivation impacts oxygen consumption in HepG2 cells, but different effects can occur. First, short-term glucose reduction can increase oxygen consumption in HepG2 cells. This suggests that the cells respond to reduced glucose levels by increasing their metabolic activity. Raman spectra (from 1 to 4 weeks) display correctly these distinct phases of proliferation, differentiation, and apoptosis. Glucose deprivation forces tumor cells to find alternative energy sources to survive. Raman spectra evidence significant modifications in lipids biocomponents: the changes of the ratio of the Raman peaks intensity ascribed to lipid deformation mode (at about 1310 cm^{-1}) to that of the Amide III band (at about 1265 cm^{-1}) suggest ROS (Reactive Oxygen Species) overproduction and consequently oxidative stress [34]. This latter is justified by the decrement of NADPH generation. Ultimately, the severe glucose deprivation in addition to hypoxia plays an additive role in increasing the expression of N-cadherin as well as Snail/Slug [35].

The expression of AFP, a key marker of hepatic differentiation, is less pronounced at three-four weeks. This observation suggests that the cells within the 3D model acquire functional characteristics specific to liver tissue, mainly due to hypoxic conditions. Hypoxia plays a role in this maturation process by modulating metabolic pathways that support cellular function in oxygen-deprived environments, a critical adaptation observed in tumor physiology. Simultaneously, we have observed that the 3 weeks cells show more intense and defined Raman peaks whose intensity decreases and downshift. Moreover, the stability of HIF-1α levels throughout the four-week culture period suggests the establishment of chronic hypoxic conditions within the 3D microenvironment: the decrement of the proliferation level occurs together a cells self-organization and differentiation into more compact spheroids [36]. This finding aligns with the behavior of solid tumours, where hypoxia critically influences cell behavior. In this respect, the collected Raman spectra show some spectral differences from those acquired in the first week, indicating a different environmental around the cells which self-organize to respond to hypoxic stimulus. A further evidence is the behavior of AFP (α-fetoprotein), an essential marker involved in pleiotropic activities affecting hepatic differentiation, which has an exponential increase at three weeks and remains stable until week 4. The role of hypoxia in stabilizing the model is not an index of structural stability but rather the occurrence of a dynamic adaptation process. Hypoxia selectively favors the survival of cells capable of thriving in low-oxygen conditions, effectively mimicking the selective pressures found in vivo. So, hypoxia is able to modulate metabolic pathways that support cell function even in oxygen-deprived environments. Particularly, the activation of one of the hypoxia-inducible factors, HIF-1α, not

Table 2
Raman bands assignment.

Raman shift (cm^{-1})	Mode	Assignment/biomolecule	Ref.
729–762	Indole ring breathing	Tryptophan – Protein	[11]
785–802	O–P–O backbone	DNA backbone, Uracil, Cytosine, Thymine – Nucleic acids	[11,24]
840–860	C–O–C skeletal mode in mono-saccharides and disaccharides	Tyrosine – Amino acid α-Glucose, Maltose, Polysaccaride structure–Carbohydrates	[11,24]
911–957	C–C stretch of proline ring	Proline, Hydroxyproline –Amino acids	[25,26]
971–988	C–C backbone	Ribose –Nucleic acid Proteins	[12]
1003–1012	CH_3 deformation or ring breathing	Phenylalanine—Protein, Carotenoids Pigment, Amino acids	[12]
1032	C–H in-plane-bending	Phenylalanine–Protein	[11]
1064–1090	Skeletal C–C stretching	Lipids, Nucleic acid	[11]
1099	Symmetric PO_2^- stretching	Nucleic acid	[11]
1122–1137	C–C stretching band	Amino acid	[27]
1170	C–H bending	Tyrosine– Amino acid	[11]
1081	Symmetric PO_2 stretching	Nucleic acid	[11]
1254–1276	C=C and H–C=C groups	Amide III–Protein Guanine and Cytosine Nucleic Acids, Lipids	[21,25,28]
1304–1324	(CH_2) twisting	Proteins, Lipids	[11]
1336–1345	ring breathing, C–H deformation mode	Adenine, Guanine –Nucleic acids, Proteins	[11]
1360–1424	CH_2 stretching, (C–H) wagging, $\delta(CH_3)$ stretching	Tryptophan– Protein	[24]
1449–1456	$\delta(CH_2)$, CH_2 bending, CH_3 deformation mode	Amide I–Protein Lipids	[21]
1578–1592	Pyrimidine ring breathing of nucleic acids	Phenylalaline–Protein Adenine, Guanine – Nucleic acid Hydroxproline – Amino acid	[11,25,26]
1598–1623	C=C bending, C–NH_2	Tryptophan,Phenylalanine–Proteins, Tyrosine– Amino acid	[11]
1656–1664	C=C stretching	Amide I–Protein Lipids	[11]

only promotes metabolic adaptations, such as aerobic glycolysis, but also regulates apoptotic processes in response to oxidative stress and reduced oxygenation [37,38]. Finally, the increase in BBC3 (apoptosis-related gene) levels at week three may indicate selective apoptosis, where less resilient cells are eliminated, allowing the more robust population to dominate the microenvironment [39]. For the cells detected at 4 weeks, all these detailed mechanisms are, in a simple way, "illustrated" by the shifting and the intensity reduction of all Raman features with respect to the 3-weeks cells. The decreased intensity of the Raman signal can be traced back to a general reduced cell vitality.

Correlation plots between the gene expression profile of the 3D HepG2 cell model and Raman spectral features at different time (Fig. 8) clearly show the evidence presented and discussed above. Each correlation plot visualizes pairwise relationships between gene expression variables and Raman spectral intensities, highlighting how specific spectral features correspond to changes in gene expression during the cellular processes in the 3D model. This approach leverages the fact that Raman spectra reflect the molecular composition and state of cells, which is influenced by their gene expression profiles and metabolic activities. By plotting these data together at various time points, temporal trends and potential linear or complex correlations can be identified between transcriptomic shifts and spectral changes, providing insights into the biochemical and structural dynamics of HepG2 cells in a 3D environment.

All these data indicates that Raman analysis can be used to assess the biochemical composition and cellular responses within HepG2 spheroids. Specifically, the main result of our Raman diagnosis is the capability to provide, for the first time to our knowledge, insights into the physiological features of the 3D HepG2 model, by detecting cell-state changes during differentiation [40]. These preliminary results have demonstrated that there is a correlation between spectral peaks and gene expression, enabling the analysis of metabolism and gene expression as a cross-network. Ultimately, Raman approach may allow to track model dynamics, long-term stability and viability as well as may facilitate earlier detection and better stratification of patients based on tumor biology.

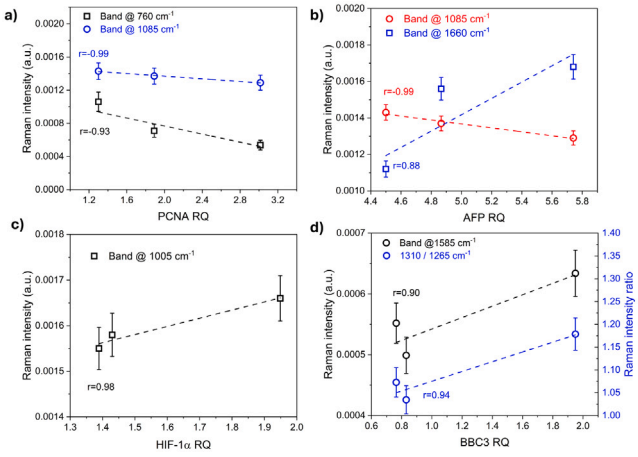

Fig. 8. Correlation plots reporting pairwise relationships between gene expression variables and Raman spectral intensities of related bands. (a) PCNA vs. Raman bands centered @ 760 and 1085 cm^{-1}; (b) AFP vs. Raman bands centered @ 1085 and 1660 cm^{-1}; (c) HIF-1α vs. Raman band centered @ 1005 cm^{-1} and (d) BBC3 vs. Raman band centered @ 1585 cm^{-1} and intensity ratio of Raman bands centered at 1310 and 1265 cm^{-1}. In every panel the Pearson's correlation coefficient, r, is reported to highlight the correlation between the considered variables.

Despite the interesting and innovative results, analyzing Raman spectra for gene expression presents still several challenges. Biological systems are composed of complex biochemicals like lipids, proteins, nucleic acids, and carbohydrates, leading to convoluted spectra where vibrations from all these components are manifested. Disentangling these overlapping signals to identify molecule-specific Raman spectral signatures is particularly difficult. Raman spectra often overlap with fluorescence, and the fluorescence background can be much more intense than the Raman bands, necessitating baseline correction and to normalize spectra. Furthermore, the choice of physical model to analyze Raman spectra is still based on the number of independent measurements. For small datasets, low-parameterized models can be

used, while large independent datasets can accommodate highly parameterized models like deep learning. In this context, ensuring independence between datasets during cross-validation or training validation is essential to avoid overestimating model performance. Thus, Raman spectroscopy is not still a direct substitute for gene expression analysis, but there needs to be an association with patterning. Despite that, this methodology, if standardized and applied routinely in hospital diagnostic laboratories, would allow hospital professionals to have, at low cost, a quick and first evidence of tumor disease for subsequent investigations with conventional and high precision biological tests. Furthermore, the same procedure could be used to monitor residual disease, thus providing useful clinical indications for patient care.

5. Conclusion

These findings collectively support the notion that the developed 3D model effectively replicates the tumor microenvironment and the importance of physiological modeling in cancer research. The presence of a stable hypoxic microenvironment seems to be crucial for driving the model evolution from an initial proliferation phase to subsequent differentiation and stabilization. Raman diagnosis provides, for the first time to our knowledge, insights into the physiological features of the 3D HepG2 model but it is not a direct substitute for gene expression analysis. Despite that, it is a potential powerful tool enabling the analysis of metabolism and gene expression as a cross-network, as preliminarily evidenced by the good correlation between Raman spectral peaks and gene expression. These evidences show that metabolic adaptations and tumor plasticity can be effectively monitored using non-invasive physical techniques.

CRediT authorship contribution statement

M.G. Rizzo: Conceptualization, Resources, Writing – review & editing. **C. Corsaro:** Visualization, Data curation, Writing – review & editing. **S. Marrara:** Investigation, Writing – review & editing. **V. Crupi:** Data curation, Writing – review & editing. **S. Conoci:** Supervision, Writing – review & editing. **F. Neri:** Supervision, Writing – review & editing. **E. Fazio:** Conceptualization, Investigation, Data curation, Writing – review & editing.

Declaration of competing interest

The authors declare that they have no known competing financial interests or personal relationships that could have appeared to influence the work reported in this paper.

Acknowledgments and funding

This work has been partially funded by European Union (NextGeneration EU), through the MUR-PNRR project SAMOTHRACE (ECS00000022).

Data availability

Data will be made available on request.

References

[1] J.M. Llovet, R.K. Kelley, A. Villanueva, A.G. Singal, E. Pikarsky, S. Roayaie, R. Lencioni, K. Koike, J. Zucman-Rossi, R.S. Finn, Hepatocellular carcinoma, Nat. Rev. Dis. Prim. 7 (1) (2021) http://dx.doi.org/10.1038/s41572-020-00240-3.

[2] R.L. Siegel, K.D. Miller, H.E. Fuchs, A. Jemal, Cancer statistics, 2022, CA: Cancer J. Clin. 72 (1) (2022) 7–33, http://dx.doi.org/10.3322/caac.21708.

[3] F. Bray, M. Laversanne, H. Sung, J. Ferlay, R.L. Siegel, I. Soerjomataram, A. Jemal, Global cancer statistics 2022: GLOBOCAN estimates of incidence and mortality worldwide for 36 cancers in 185 countries, CA: Cancer J. Clin. 74 (3) (2024) 229–263, http://dx.doi.org/10.3322/caac.21834.

[4] D.F. Quail, J.A. Joyce, Microenvironmental regulation of tumor progression and metastasis, Nature Med. 19 (11) (2013) 1423–1437, http://dx.doi.org/10.1038/nm.3394.

[5] O. Urzì, R. Gasparro, E. Costanzo, A. De Luca, G. Giavaresi, S. Fontana, R. Alessandro, Three-dimensional cell cultures: The bridge between in Vitro and in Vivo models, Int. J. Mol. Sci. 24 (15) (2023) 12046, http://dx.doi.org/10.3390/ijms241512046.

[6] F. Urciuolo, G. Imparato, P.A. Netti, In vitro strategies for mimicking dynamic cell–ECM reciprocity in 3D culture models, Front. Bioeng. Biotechnol. 11 (2023) http://dx.doi.org/10.3389/fbioe.2023.1197075.

[7] J. Rodrigues, M.A. Heinrich, L.M. Teixeira, J. Prakash, 3D in vitro model (r)evolution: Unveiling Tumor–Stroma interactions, Trends Cancer 7 (3) (2021) 249–264, http://dx.doi.org/10.1016/j.trecan.2020.10.009.

[8] A. Al Hrout, K. Cervantes-Gracia, R. Chahwan, A. Amin, Modelling liver cancer microenvironment using a novel 3D culture system, Sci. Rep. 12 (1) (2022) http://dx.doi.org/10.1038/s41598-022-11641-7.

[9] M. Štampar, B. Breznik, M. Filipič, B. Žegura, Characterization of in vitro 3D cell model developed from human hepatocellular carcinoma (HepG2) cell line, Cells 9 (12) (2020) 2557, http://dx.doi.org/10.3390/cells9122557.

[10] G. Bordanaba-Florit, I. Madarieta, B. Olalde, J.M. Falcón-Pérez, F. Royo, 3D cell cultures as prospective models to study extracellular vesicles in cancer, Cancers 13 (2) (2021) 307, http://dx.doi.org/10.3390/cancers13020307.

[11] C. Esposito, M. Janneh, S. Spaziani, V. Calcagno, M.L. Bernardi, M. Iammarino, C. Verdone, M. Tagliamonte, L. Buonaguro, M. Pisco, L. Aversano, A. Cusano, Assessment of primary human liver cancer cells by artificial intelligence-assisted Raman spectroscopy, Cells 12 (22) (2023) 2645, http://dx.doi.org/10.3390/cells12222645.

[12] L. Huang, H. Sun, L. Sun, K. Shi, Y. Chen, X. Ren, Y. Ge, D. Jiang, X. Liu, W. Knoll, Q. Zhang, Y. Wang, Rapid, label-free histopathological diagnosis of liver cancer based on Raman spectroscopy and deep learning, Nat. Commun. 14 (1) (2023) http://dx.doi.org/10.1038/s41467-022-35696-2.

[13] C. Esposito, M. Janneh, S. Spaziani, V. Calcagno, M.L. Bernardi, M. Iammarino, C. Verdone, M. Tagliamonte, L. Buonaguro, M. Pisco, L. Aversano, A. Cusano, Artificial intelligence-assisted Raman spectroscopy for liver cancer diagnosis, in: L. De Stefano, R. Velotta, E. Descrovi (Eds.), EPJ Web Conf. 309 (2024) 10010, http://dx.doi.org/10.1051/epjconf/202430910010.

[14] M. Shri, H. Agrawal, P. Rani, D. Singh, S.K. Onteru, Hanging drop, a best three-dimensional (3D) culture method for primary buffalo and sheep hepatocytes, Sci. Rep. 7 (1) (2017) http://dx.doi.org/10.1038/s41598-017-01355-6.

[15] M. Rasouli, F. Safari, M.H. Kanani, H. Ahvati, Principles of hanging drop method (spheroid formation) in cell culture, in: Autophagy in Development and Disease, Springer US, 2024, pp. 289–300, http://dx.doi.org/10.1007/7651_2024_527.

[16] S. Costantini, G. Di Bernardo, M. Cammarota, G. Castello, G. Colonna, Gene expression signature of human HepG2 cell line, Gene 518 (2) (2013) 335–345, http://dx.doi.org/10.1016/j.gene.2012.12.106.

[17] M. Bokhari, R.J. Carnachan, N.R. Cameron, S.A. Przyborski, Culture of HepG2 liver cells on three dimensional polystyrene scaffolds enhances cell structure and function during toxicological challenge, J. Anat. 211 (4) (2007) 567–576, http://dx.doi.org/10.1111/j.1469-7580.2007.00778.x.

[18] M. Banihashemi, M. Mohkam, A. Safari, N. Nezafat, M. Negahdaripour, F. Mohammadi, S. Kianpour, Y. Ghasemi, Optimization of three dimensional culturing of the HepG2 cell line in fibrin scaffold, Hepat. Mon. 15 (3) (2015) http://dx.doi.org/10.5812/hepatmon.22731.

[19] T.-M. Achilli, J. Meyer, J.R. Morgan, Advances in the formation, use and understanding of multi-cellular spheroids, Expert. Opin. Biol. Ther. 12 (10) (2012) 1347–1360, http://dx.doi.org/10.1517/14712598.2012.707181.

[20] C. Ma, L. Zhang, T. He, H. Cao, X. Ren, C. Ma, J. Yang, R. Huang, G. Pan, Single cell Raman spectroscopy to identify different stages of proliferating human hepatocytes for cell therapy, Stem Cell Res. Ther. 12 (1) (2021) http://dx.doi.org/10.1186/s13287-021-02619-9.

[21] P.N. Paramitha, R. Zakaria, A. Maryani, Y. Kusaka, B.B. Andriana, K. Hashimoto, H. Nakazawa, S. Kato, H. Sato, Raman study on lipid droplets in hepatic cells co-cultured with fatty acids, Int. J. Mol. Sci. 22 (14) (2021) 7378, http://dx.doi.org/10.3390/ijms22147378.

[22] A. Wang, W. Ruan, W. Song, L. Chen, B. Zhao, Y.M. Jung, X. Wang, Detection of the potential tumor marker of AFP using surface-enhanced Raman scattering-based immunoassay, J. Raman Spectrosc. 44 (12) (2013) 1649–1653, http://dx.doi.org/10.1002/jrs.4391.

[23] K.-C. Huang, J. Li, C. Zhang, Y. Tan, J.-X. Cheng, Multiplex stimulated Raman scattering imaging cytometry reveals lipid-rich protrusions in cancer cells under stress condition, IScience 23 (3) (2020) 100953, http://dx.doi.org/10.1016/j.isci.2020.100953.

[24] M. Bonsignore, S. Trusso, C. De Pasquale, G. Ferlazzo, A. Allegra, V. Innao, C. Musolino, D. Franco, L. Maria De Plano, S.P.P. Guglielmino, F. Neri, E. Fazio, A multivariate analysis of multiple myeloma subtype plasma cells, Spectrochim. Acta Part A: Mol. Biomol. Spectrosc. 258 (2021) 119813, http://dx.doi.org/10.1016/j.saa.2021.119813.

[25] M. Gargotti, E. Efeoglu, H.J. Byrne, A. Casey, Raman spectroscopy detects biochemical changes due to different cell culture environments in live cells in vitro, Anal. Bioanal. Chem. 410 (28) (2018) 7537–7550, http://dx.doi.org/10.1007/s00216-018-1371-5.

[26] N. Stone, C. Kendall, J. Smith, P. Crow, H. Barr, Raman spectroscopy for identification of epithelial cancers, Faraday Discuss. 126 (2004) 141, http://dx.doi.org/10.1039/b304992b.

[27] O. Ryabchykov, K. Bräutigam, K. Galler, U. Neugebauer, A. Mosig, T. Bocklitz, J. Popp, Raman spectroscopic investigation of the human liver stem cell line heparg, J. Raman Spectrosc. 49 (6) (2018) 935–942, http://dx.doi.org/10.1002/jrs.5392.

[28] T. Tolstik, C. Marquardt, C. Matthäus, N. Bergner, C. Bielecki, C. Krafft, A. Stallmach, J. Popp, Discrimination and classification of liver cancer cells and proliferation states by Raman spectroscopic imaging, Analyst 139 (22) (2014) 6036–6043, http://dx.doi.org/10.1039/c4an00211c.

[29] S. Uxa, P. Castillo-Binder, R. Kohler, K. Stangner, G.A. Müller, K. Engeland, Ki-67 gene expression, Cell Death Differ. 28 (12) (2021) 3357–3370, http://dx.doi.org/10.1038/s41418-021-00823-x.

[30] S. Roy, S. Kumaravel, A. Sharma, C.L. Duran, K.J. Bayless, S. Chakraborty, Hypoxic tumor microenvironment: Implications for cancer therapy, Exp. Biol. Med. 245 (13) (2020) 1073–1086, http://dx.doi.org/10.1177/1535370220934038.

[31] L.-f. WU, G.-p. LI, J.-l. FENG, Z.-j. PU, Molecular mechanisms of adenosine-induced apoptosis in human HepG2 cells, Acta Pharmacol. Sin. 27 (4) (2006) 477–484, http://dx.doi.org/10.1111/j.1745-7254.2006.00302.x.

[32] E. Elje, E. Mariussen, O.H. Moriones, N.G. Bastús, V. Puntes, Y. Kohl, M. Dusinska, E. Rundén-Pran, Hepato(geno)toxicity assessment of nanoparticles in a HepG2 liver spheroid model, Nanomaterials 10 (3) (2020) 545, http://dx.doi.org/10.3390/nano10030545.

[33] A. Venturi, F.D. Piaz, C. Giovannini, L. Gramantieri, P. Chieco, L. Bolondi, Human hepatocellular carcinoma expresses specific PCNA isoforms: an in vivo and in vitro evaluation, Lab. Invest. 88 (9) (2008) 995–1007, http://dx.doi.org/10.1038/labinvest.2008.50.

[34] E. Fazio, A. Speciale, S. Spadaro, M. Bonsignore, F. Cimino, M. Cristani, D. Trombetta, A. Saija, F. Neri, Evaluation of biological response induced by molybdenum oxide nanocolloids on in vitro cultured NIH/3T3 fibroblast cells by micro-Raman spectroscopy, Colloids Surf. B 170 (2018) 233–241, http://dx.doi.org/10.1016/j.colsurfb.2018.06.028.

[35] H. Jo, J. Lee, J. Jeon, S.y. Kim, J.-i. Chung, H.y. Ko, M. Lee, M. Yun, The critical role of glucose deprivation in epithelial-mesenchymal transition in hepatocellular carcinoma under hypoxia, Sci. Rep. 10 (1) (2020) http://dx.doi.org/10.1038/s41598-020-58124-1.

[36] S.C. Ramaiahgari, M.W. den Braver, B. Herpers, V. Terpstra, J.N.M. Commandeur, B. van de Water, L.S. Price, A 3D in vitro model of differentiated HepG2 cell spheroids with improved liver-like properties for repeated dose high-throughput toxicity studies, Arch. Toxicol. (2014) http://dx.doi.org/10.1007/s00204-014-1215-9.

[37] J. Mathieu, W. Zhou, Y. Xing, H. Sperber, A. Ferreccio, Z. Agoston, K.T. Kuppusamy, R.T. Moon, H. Ruohola-Baker, Hypoxia-inducible factors have distinct and stage-specific roles during reprogramming of human cells to pluripotency, Cell Stem Cell 14 (5) (2014) 592–605, http://dx.doi.org/10.1016/j.stem.2014.02.012.

[38] M. Li, H. Li, C. Li, S. Wang, W. Jiang, Z. Liu, S. Zhou, X. Liu, M.A. McNutt, G. Li, Alpha-fetoprotein: A new member of intracellular signal molecules in regulation of the PI3K/AKT signaling in human hepatoma cell lines, Int. J. Cancer 128 (3) (2010) 524–532, http://dx.doi.org/10.1002/ijc.25373.

[39] K. Nakano, K.H. Vousden, PUMA, a novel proapoptotic gene, is induced by p53, Mol. Cell 7 (3) (2001) 683–694, http://dx.doi.org/10.1016/s1097-2765(01)00214-3.

[40] T.M. Watanabe, K. Sasaki, H. Fujita, Recent advances in Raman spectral imaging in cell diagnosis and gene expression prediction, Genes 13 (11) (2022) 2127, http://dx.doi.org/10.3390/genes13112127.